

Musculoskeletal AutoEncoder: A Unified Online Acquisition Method of Intersensory Networks for State Estimation, Control, and Simulation of Musculoskeletal Humanoids

Kento Kawaharazuka¹, Kei Tsuzuki¹, Moritaka Onitsuka¹, Yuki Asano¹
Kei Okada¹, Koji Kawasaki², and Masayuki Inaba¹

Abstract—While the musculoskeletal humanoid has various biomimetic benefits, the modeling of its complex structure is difficult, and many learning-based systems have been developed so far. There are various methods, such as control methods using acquired relationships between joints and muscles represented by a data table or neural network, and state estimation methods using Extended Kalman Filter or table search. In this study, we construct a Musculoskeletal AutoEncoder representing the relationship among joint angles, muscle tensions, and muscle lengths, and propose a unified method of state estimation, control, and simulation of musculoskeletal humanoids using it. By updating the Musculoskeletal AutoEncoder online using the actual robot sensor information, we can continuously conduct more accurate state estimation, control, and simulation than before the online learning. We conducted several experiments using the musculoskeletal humanoid Musashi, and verified the effectiveness of this study.

I. INTRODUCTION

The musculoskeletal humanoid [1]–[4] has many biomimetic benefits such as muscle redundancy, variable stiffness control with nonlinear elastic elements, joint torque control with cheap muscle tension sensors, and the flexible under-actuated fingers and spine. On the other hand, its complex musculoskeletal structure is difficult to modelize, and applying conventional control methods is challenging.

To solve this problem, many learning-based systems have been developed so far. In this study, we mainly handle the state estimation, control, and simulation methods of musculoskeletal humanoids. The state estimation is to estimate joint angle from muscle length and muscle tension, the control is to calculate target muscle length from target joint angle and torque, and the simulation is to simulate the transition of joint angle and muscle tension from target muscle length and external force. We summarize these studies that especially handle the actual robot in Fig. 1.

First, because the musculoskeletal humanoid typically does not have joint angle sensors due to complex joints, such as the scapula and shoulder ball joints, several methods have been developed to estimate joint angles. Ookubo, et al. have trained a nonlinear relationship between joint angles and muscle lengths (joint-muscle mapping, JMM), represented by

	State Estimation	Control	Simulation
Polynomials	Ookubo, et al.		
Data Table	Nakanishi, et al.	Motegi, et al.	
Neural Network	Ookubo, et al.	Mizuuchi, et al.	Offline Learning
	+ anomaly detection	Kawaharazuka, et al.	Online Learning
	This Study		

Fig. 1. Classification of previous studies and positioning of this study.

polynomials, using inertial measurement sensors (IMU), and estimated joint angles using the polynomials and Extended Kalman Filter (EKF) [5]. Nakanishi, et al. have constructed a data table representing JMM, and estimated the joint angles using muscle length sensors and table search algorithm [6]. JMMs used in these methods are trained offline. Also, the method proposed by Ookubo, et al. can be applied to JMM represented by a neural network.

Second, we will explain several learning-based control methods. Motegi, et al. have constructed a data table associating the position of end effectors and muscle lengths, and proposed a method to realize the accurate position of the end effectors [7]. Mizuuchi, et al. have controlled the robot by training JMM represented by a neural network using motion capture data [8]. Kawaharazuka, et al. have developed a control method with JMM updated online using the actual robot sensor information [9], and developed an extended control method considering the musculoskeletal body tissue softness [10], [11]. Although there are several control methods using reinforcement learning [12], they are difficult to use for the actual robot. Also, there are no studies applying learning-based methods to not only state estimation and control but also simulation of the musculoskeletal structure. We need to make the simulator closer to the actual robot by learning. On the other hand, there are several simulations using geometric models [13]–[15].

In this study, we propose a Musculoskeletal AutoEncoder (MAE) uniformly handling the state estimation, control, and simulation of musculoskeletal humanoids. By updating MAE online using the actual robot sensor information, we can continuously conduct more accurate state estimation, control, and simulation of the musculoskeletal structure than before the online learning. This study only handles quasi-static states, and does not consider dynamic states. Also, we

¹ The author are associated with Department of Mechano-Informatics, Graduate School of Information Science and Technology, The University of Tokyo. {kawaharazuka, tsuzuki, onitsuka, asano, k-okada, inaba}@jsk.t.u-tokyo.ac.jp

² The author is associated with TOYOTA MOTOR CORPORATION. koji_kawasaki@mail.toyota.co.jp

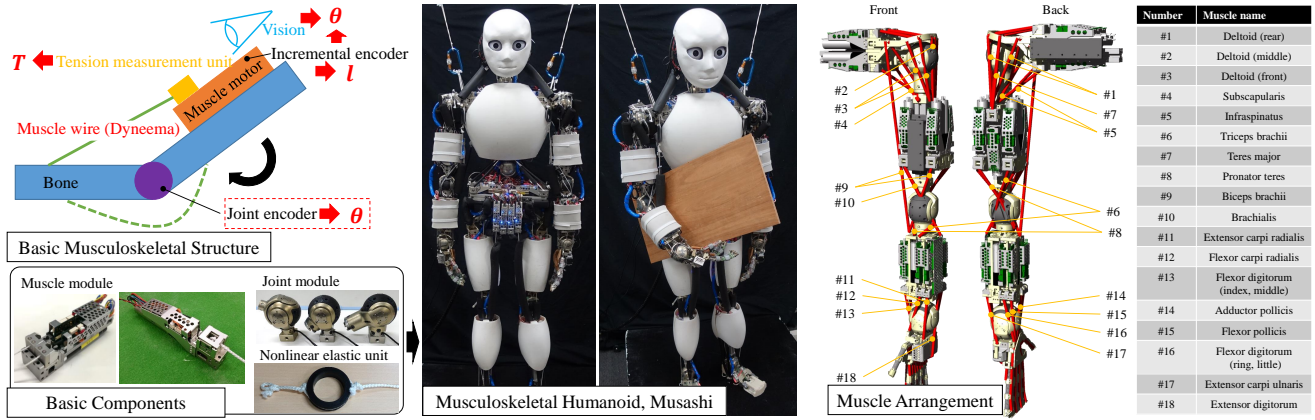


Fig. 2. The basic structure of musculoskeletal humanoids covered in this study, and the musculoskeletal humanoid Musashi used in this study.

assume that the geometric model, including joint position, link length, and link weight, is correct.

II. MUSCULOSKELETAL HUMANOIDS AND INTERSENSORY NETWORKS

A. Musculoskeletal Humanoids

The musculoskeletal humanoid covered in this study has a musculoskeletal structure mimicking human joints and muscles [1]–[4]. Compared to the tendon-driven robot with constant moment arms of muscles to joints [16], [17] which is easy to modelize, these robots are difficult to modelize because the moment arms change complexly depending on the posture. We show the basic structure of musculoskeletal humanoids in the upper left figure of Fig. 2. Muscles are antagonistically arranged around joints, and muscle length l , muscle tension T , and muscle temperature C of each muscle can be measured. Dyneema, which is a chemical fiber resistant to friction, is used for each muscle and it slightly elongates depending on muscle tension. Depending on the robot, there are nonlinear elastic elements at the ends of muscles in order to enable variable stiffness control. Also, although some robots have sensors to measure joint angles θ [18], [19], ordinary musculoskeletal humanoids do not have these sensors due to complex joint structures such as ball joints and the scapula, and so joint angles cannot be directly measured. However, the actual joint angles can be estimated by using vision sensor attached to the head [9]. In this method, an AR marker is attached to the robot end effector, e.g. the hand, to obtain the posture P_{marker} , and Inverse Kinematics is solved to $P_{target} = P_{marker}$ by setting the initial joint angles $\theta_{initial}$ as the estimated joint angles $\theta_{current}^{estimated}$ from the change in muscle lengths [5], as shown below,

$$\theta_{current}^{estimated'} = \text{IK}(P_{target} = P_{marker}, \theta_{initial} = \theta_{current}^{estimated}) \quad (1)$$

where IK means Inverse Kinematics, and $\theta_{current}^{estimated'}$ is the estimated actual joint angles compensated for by vision sensor. There are other sensors such as IMUs, tactile sensors, etc.

We show the musculoskeletal humanoid Musashi [18] used for experiments of this study in the center figure of Fig. 2,

and show the muscle arrangement of its left arm in the right figure of Fig. 2. Musashi is mainly composed of the muscle modules, joint modules, nonlinear elastic elements shown in the lower left figure of Fig. 2. The joint modules enabling the measurement of joint angles advance our investigation of learning control systems, and nonlinear elastic elements enable soft contact with the environment and variable stiffness control. In this study, we mainly handle the 3 degrees of freedom (DOFs) shoulder and 2 DOFs elbow, and we represent these joint angles as $\theta = (\theta_{S-r}, \theta_{S-p}, \theta_{S-y}, \theta_{E-p}, \theta_{E-y})$ (S means the shoulder, E means the elbow, and rpy means the roll, pitch, and yaw, respectively). Also, 10 muscles are related to these 5 DOFs.

B. Musculoskeletal Intersensory Networks

In this study, among the introduced sensors, we focus on the joint angle θ , muscle tension T , and muscle length l which can be definitely measured and have strong correlations. In previous studies [8], [9], the nonlinear relationship between θ and l : $\theta \rightarrow l$ is trained. By extending them and considering the body tissue softness specific to the musculoskeletal structure, the relationship of $(\theta, T) \rightarrow l$ is trained in [10], [11].

In actuality, there exist relationships of not only ① $(\theta, T) \rightarrow l$ but also ② $(T, l) \rightarrow \theta$ and ③ $(\theta, l) \rightarrow T$. Thus, among (θ, T, l) , one sensor value can be calculated from the other two. In other words, all of the sensor information can be calculated from two sensor values.

Of course, other sensors such as vision and tactile information will be able to be incorporated in the future.

III. MUSCULOSKELETAL AUTOENCODER

A. Network Structure and System Overview

First, we show the network structure of MAE in Fig. 3. MAE is a simple AutoEncoder-type network [20] whose inputs are (θ, T, l) and $mask$, and whose output is (θ, T, l) . The dimension of $(\theta, T, l, mask)$ is $(D, M, M, 3)$ (D is the number of joint angles, M is the number of muscles, and $mask$ has 3 binarized values). We represent the middle layer of MAE, whose dimension is the lowest, as z , and its dimension is $D + M$. The reason is that the dimension of z can be reduced to less than $D + M$ because (θ, T, l)

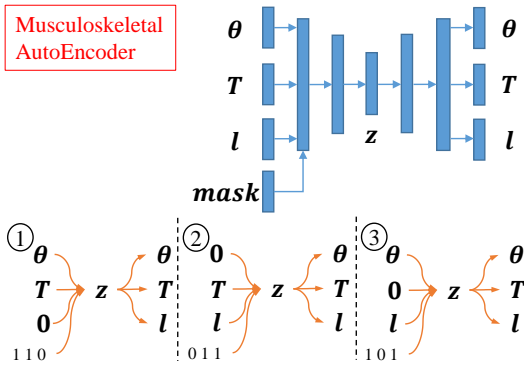


Fig. 3. The network structure of Musculoskeletal AutoEncoder.

can be inferred from (θ, T) , $D+M$ dimension. In this study, MAE is composed of 7 layers including its input and output layers, and the numbers of units are $(D+2M+3, 200, 30, D+M, 30, 200, D+2M)$. The number of layers do not largely affect the final inference accuracy, but the inference accuracy decreases with less number of units in the hidden layers than this configuration. Also, in order to align the scales of (θ, T, l) , we set their units as ([rad], [N/200], [mm/100]).

Second, we will explain the overview of initial training and online learning of MAE. Although the structure of MAE is similar to an ordinary AutoEncoder, its training method is specific. As stated in Section II-B, we make use of the characteristic that all 3 sensor values (θ, T, l) can be obtained from two among them. Thus, in the case only (θ, T) can be obtained, like ① shown in Fig. 3, MAE outputs (θ, T, l) from the input of $(\theta, T, 0, (1, 1, 0))$. In the beginning, we conduct initial training of MAE from the geometric model including the relationship between joint angles and muscle lengths. Next, we update MAE online using the actual robot sensor information.

We represent the encoder part of MAE as $z = f_{encode}(\theta, T, l, mask)$ and the decoder part of MAE as $(\theta, T, l) = f_{decode}(z)$. Also, we represent f_{encode} of ① as $f_{encode,1}(\theta, T) = f_{encode}(\theta, T, 0, (1, 1, 0))$, that of ② as $f_{encode,2}(T, l) = f_{encode}(0, T, l, (0, 1, 1))$, and that of ③ as $f_{encode,3}(\theta, l) = f_{encode}(\theta, 0, l, (1, 0, 1))$. Regarding the decoder, we represent $\theta = f_{decode,\theta}(z)$, $T = f_{decode,T}(z)$, and $l = f_{decode,l}(z)$.

We show the whole system using this MAE in Fig. 4. By using MAE and its backpropagation, we can conduct state estimation, control, and simulation of musculoskeletal humanoids.

B. Initial Training

We will explain the initial training of MAE using a geometric model. In the geometric model, each muscle route is represented by linearly connecting its start point, relay points, and end point. By setting a certain joint angle, muscle length can be calculated from the distance of the start, relay, and end points. In this study, we represent a function calculating the absolute muscle length from the geometric model as $f_{geo,abs}(\theta)$, and represent a function calculating the muscle length relative to the length at the initial posture (all

the joint angles are 0, $\theta = 0$) as $f_{geo}(\theta)$.

First, we estimate the relationship between muscle tension T and muscle length elongation including nonlinear elastic elements $L_e(l_{abs}, T)$ considering the elongation of Dyneema, which is proportional to the absolute muscle length l_{abs} , from a testbed of one muscle. Second, we generate the data as shown below,

$$(\theta, T, l) = (\theta_r, T_r, f_{geo}(\theta_r) - L_e(f_{geo,abs}(\theta_r), T_r)) \quad (2)$$

where θ_r is random joint angle, and T_r is random muscle tension. Using this data, we randomly execute ①, ②, and ③ shown in Fig. 3. Thus, we randomly set one element among (θ, T, l) as 0, input the corresponding *mask* into MAE, and output $(\theta_{calc}, T_{calc}, l_{calc})$. Finally, we calculate the loss $L_{initial}$ as shown below, and train MAE,

$$L_{initial} = w_\theta \|\theta - \theta_{calc}\|_2 + w_T \|T - T_{calc}\|_2 + w_l \|l - l_{calc}\|_2 \quad (3)$$

where $\|\cdot\|_2$ represents L2 norm.

In this study, we set the number of batches for initial training $C_{batch}^{initial} = 100$, the number of epochs $C_{epoch}^{initial} = 30$, $w_\theta = 1.0$, $w_T = 10.0$, and $w_l = 10.0$. Also, we use Adam [21] as the optimization method of MAE.

C. Online Learning

We will explain the online learning method of MAE using the actual robot sensor information.

First, the sensor values of $(\theta_{current}, T_{current}, l_{current})$ are accumulated from the actual robot. If joint angles cannot be directly measured, $\theta_{current}^{estimated}$ in Section II-A is used as $\theta_{current}$. The data is accumulated when the current joint angle or muscle tension deviates from the previously accumulated data by more than a certain threshold, and the robot is not moving. MAE begins to be updated when the number of the accumulated data exceeds C_{thre} . A batch for online learning is constructed using the newest data, $(0, 0, 0)$, and randomly chosen C_{data} ($C_{data} \leq C_{thre}$) number of data from the accumulated data. Then, 3 kinds of *mask* of ①, ②, and ③ are added to each data in the batch. Finally, MAE is updated using the batch with $3 \times (C_{data} + 2)$ number of data in total.

In this study, we set the number of batches for online learning $C_{batch}^{online} = 10$, the number of epochs $C_{epoch}^{online} = 10$, $C_{thre} = 20$, and $C_{data} = 10$.

D. State Estimation Using Musculoskeletal AutoEncoder

We will explain the state estimation method of musculoskeletal humanoids using the trained MAE. As stated in Section II-A, the ordinary musculoskeletal humanoid [4] does not have joint angle sensors, and so the actual joint angles are estimated using vision information. However, in this case, an AR marker has to be attached to the robot, and the robot must keep watching its body to know the current joint angles. By estimating joint angles from the current muscle length and muscle tension information, the robot can know the self-body state continuously.

best γ at each step is chosen for better optimization. We decide a maximum value of γ as $\gamma_{max}^{control}$, divide $[0, \gamma_{max}^{control}]$ equally into $N_{batch}^{control}$ parts, and generate $N_{batch}^{control}$ number of z updated by these γ . 1) and 2) are executed again, and z with the lowest $L_{control}$ is used. These procedures are repeated $C_{epoch}^{control}$ times. Then $(\theta_{calc}, T_{calc}, l_{calc}) = f_{dec}(z)$ is calculated. Finally l_{target} is calculated from the obtained l_{calc}, T_{calc} as shown below, and is sent to the actual robot.

$$l_{target} = l_{calc} + l_{comp}(T_{calc}) \quad (12)$$

By using this method, l_{target} with minimized muscle tension can be obtained, while realizing θ_{target} . Although we can directly calculate $T_{target} = T_{calc}$ by quadratic programming minimizing $\|T_{target}\|_2$ and fulfilling $\tau_{target} = -G^T T_{target}$, there is no guarantee that T_{target} can be realized at the posture of θ_{target} , and so we search T_{target} and l_{target} in the acquired latent space of z .

Third, we will explain the method of muscle tension-based control and variable stiffness control. Because only muscle Jacobian is required for muscle tension-based controls, we obtain G as stated above, and can conduct these controls as in [24]. Also, we can conduct variable stiffness control as in [11] by using $f_{encode,1}(\theta, T)$.

In this study, we set $w_1 = 1.0, w_2 = 1.0, w_3 = 0.01, \gamma_{max}^{control} = 0.5, C_{batch}^{control} = 10,$ and $C_{epoch}^{control} = 10$.

F. Simulation Using Musculoskeletal AutoEncoder

We will explain the simulation method of the musculoskeletal humanoid using MAE. We simulate the transition of joint angles and muscle tensions by commanding muscle lengths.

First, the state of latent space $z = f_{encode,2}(T_{sim}, l_{sim})$ is calculated from the current muscle tension T_{sim} and length l_{sim} in the current simulation. Second, the procedures of 1)–3) are repeated as in Section III-E. The difference is only the calculation of loss in 2). In the following explanations, we substitute $L_{sim,1}$ or $L_{sim,2}$ for the $L_{control}$ in Section III-E. The loss of $L_{sim,1}$ is calculated as shown below,

$$L_{sim,1}(\theta, T, l) = w_4 \|T\|_2 + w_5 \|l - l_{sim}\|_2 + w_6 \|\tau_{target} + G^T(\theta_{sim}, T_{sim})T\|_2 \quad (13)$$

By using this loss, the state of latent space z , which fulfills the current muscle length and generates the joint torque τ_{target} required for gravity compensation, can be obtained. When we would like to simulate motions when applying external force, we calculate the necessary torque from the geometric model, and conduct the simulation similarly. Also, by changing the loss L , we can simulate not only external force, but also motions when changing to a certain posture θ_{fix} forcibly, when resting the arms on the table, etc. In this case, the loss of $L_{sim,2}$ is calculated as shown below,

$$L_{sim,2}(\theta, T, l) = w_4 \|T\|_2 + w_5 \|l - l_{sim}\|_2 + w_7 \|\theta - \theta_{fix}\|_2 \quad (14)$$

When using this loss, the simulator works more stably by changing the calculation of z to $z = f_{encode,3}(\theta_{sim}, l_{sim})$.

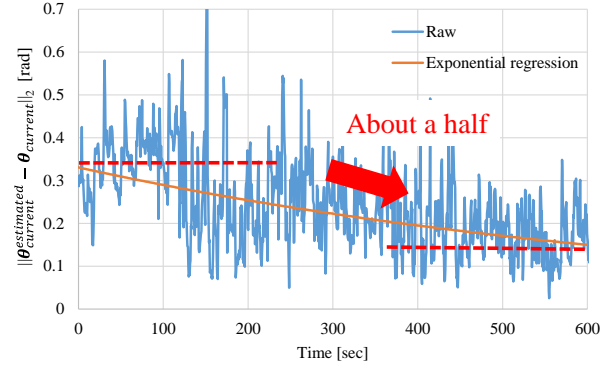


Fig. 5. The transition of the error between the current and estimated joint angles while executing online learning of Musculoskeletal AutoEncoder.

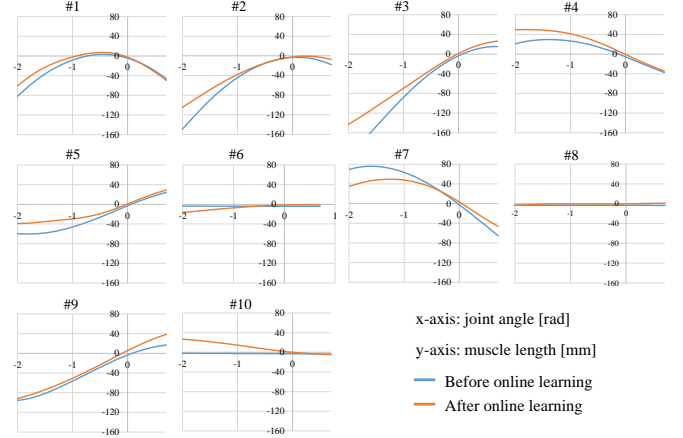


Fig. 6. The transition of muscle lengths by changing joint angles in Musculoskeletal AutoEncoder, before and after the online learning.

Finally, we obtain $(\theta'_{sim}, T'_{sim}, l'_{sim}) = f_{decode}(z)$ from the calculated z , and update the simulator by setting $\theta_{sim} = \theta'_{sim}$ and $T_{sim} = T'_{sim}$. We can conduct simulation of the musculoskeletal humanoid by executing these procedures real-time.

In this study, we set $w_4 = 0.1, w_5 = 1.0, w_6 = 0.001, w_7 = 1.0, \gamma_{max}^{sim} = 0.2, C_{batch}^{sim} = 10,$ and $C_{epoch}^{sim} = 3 \gamma_{max}^{sim}, C_{batch}^{sim}$, and C_{epoch}^{sim} mean $\gamma_{max}^{control}, C_{batch}^{control},$ and $C_{epoch}^{control}$ for simulation, respectively.

IV. EXPERIMENTS

As stated in Section II-A, we mainly use the 5 DOFs joints of the shoulder and elbow for the evaluation of this study, and so we set $D = 5$ and $M = 10$.

A. Online Learning of Musculoskeletal AutoEncoder

We conducted an experiment regarding the online learning of MAE. In this study, we moved the robot by 3 steps as in [11] and updated MAE. First, we conducted Eq. 7 over 5 sec by setting target joint angle θ_{target} randomly and setting T_{const} as T_{bias} . Second, we conducted Eq. 8 over 2 sec with the same θ_{target} . Third, we conducted Eq. 7 over 3 sec again by setting T_{const} randomly in the range of $[T_{bias}, T_{limit}]$. By repeating these 3 steps, the multidimensional space of joint

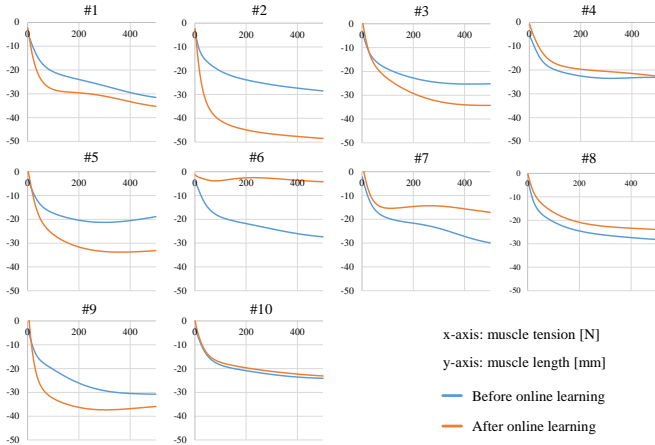


Fig. 7. The transition of muscle lengths by changing muscle tensions in Musculoskeletal AutoEncoder, before and after the online learning.

angles and muscle tensions in MAE is efficiently updated. In these steps, we set $T_{bias} = 30$ [N] and $T_{limit} = 200$ [N].

We show the transition of the difference between the estimated joint angles $\theta_{current}^{estimated}$ and values of joint angle sensors $\theta_{current}$, $\|\theta_{current}^{estimated} - \theta_{current}\|_2$, in Fig. 5. During online learning, $\|\theta_{current}^{estimated} - \theta_{current}\|_2$ gradually decreased. From the exponential approximation of 10 minutes, we can see that the error of joint angle estimation decreased by about half after 10 minutes, from 0.324 [rad] to 0.154 [rad] on average. The error of $\|\theta_{current}^{estimated} - \theta_{current}\|_2$ remained, and it is considered to be due to muscle hysteresis caused by friction of joints and muscles. This study can only consider quasi-static movements and cannot consider dynamics-related errors such as hysteresis.

We show the change of MAE before and after the online learning in Fig. 6 and Fig. 7. In Fig. 6, we show the change in muscle lengths when setting muscle tension as $\mathbf{0}$ and changing θ_{S-p} in the range of $[-120, 30]$ [deg]. In Fig. 7, we show the change in muscle lengths when changing muscle tension in the range of $[0, 500]$ [N] at the initial posture. Both of the graphs change largely after online learning. Muscle lengths in Fig. 6 changed up to about 40 [mm] while passing the origin. Especially, the changes in muscle lengths of the major muscles that move θ_{S-p} , e.g. #2, #3, and #7 in Fig. 2, are large. Also, muscles in Fig. 7 expressed various characteristics of linearity, e.g. #2, and nonlinearity, e.g. #6. Because #2 is a muscle which large tension is often applied to, the characteristic of the nonlinear elastic unit changed largely. Also, because #6 is a muscle of the elbow joint and the friction is large due to its muscle route, the nonlinearity vanished.

B. State Estimation Using Musculoskeletal AutoEncoder

We conducted an experiment of state estimation using MAE. We sent the same motions to the robot before and after online learning. In the middle of the experiment, the robot grasped a heavy object (3.6 kg dumbbell), and then we deactivated the muscle #2 shown in Fig. 2. We evaluated the tracking ability of the estimated joint angles and the value A

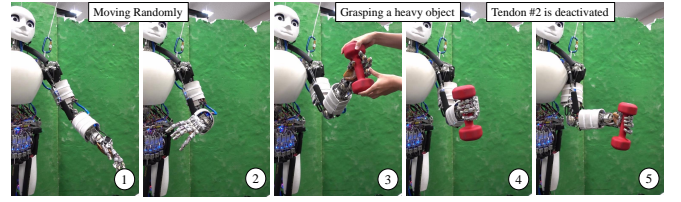


Fig. 8. The experiment of state estimation using Musculoskeletal AutoEncoder.

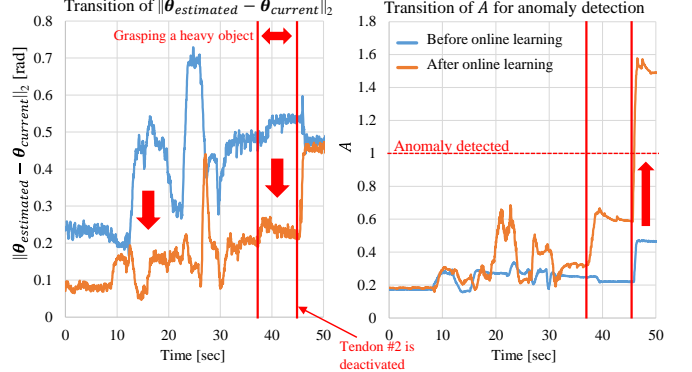


Fig. 9. The result of state estimation using Musculoskeletal AutoEncoder.

for anomaly detection before and after online learning. We did not conduct online learning during the motions. We show the experiment in Fig. 8, and its result in Fig. 9.

When moving randomly, the error of the estimated joint angles largely decreased after online learning from 0.414 [rad] to 0.186 [rad] on average. The space of muscle tension is efficiently learned during online learning, and the error did not change significantly when grasping the heavy dumbbell. In the case before online learning, the change in error also seems small because the error was originally high. Next, we will examine the transition of A . After online learning, A rapidly rose when deactivating muscle #2 and we can detect anomaly well. On the other hand, A did not rise very much before online learning. This is considered to be because we set muscle tension randomly at initial training, and MAE is trained to restore the input value even when setting muscle tension impossible at that posture.

C. Control Using Musculoskeletal AutoEncoder

We conducted experiments regarding joint angle control using MAE. First, we decided 5 random joint angles θ_{eval} for evaluation. We moved the robot from the random joint angle θ_{random} to θ_{eval} 5 times while changing θ_{random} , and evaluated the average and variance of $\|\theta_{eval} - \theta_{current}\|_2$ and $\|T_{current}\|_2$. We conducted the experiment in this way to consider the effect of muscle hysteresis. We show the result of moving the robot using the geometric model (**geometric**), using Eq. 7 (**first**) and Eq. 8 (**second**) in order after online learning, and using Eq. 12 after online learning (**proposed**) in Fig. 10.

From the result, we can see that the precision using controls after online learning (**first**, **second**, and **proposed**) were much better than that using the geometric model

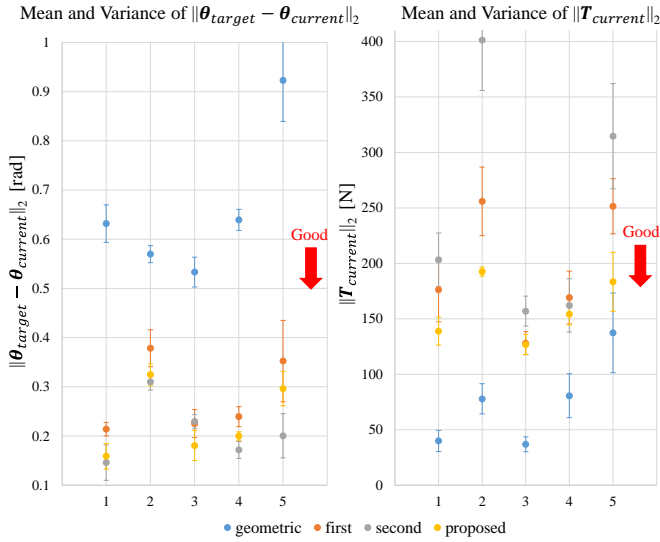


Fig. 10. The average and variance of $\|\theta_{eval} - \theta_{current}\|_2$ and $\|T_{current}\|_2$ among four controls: **geometric**, **first**, **second**, and **proposed**.

(**geometric**). Also, the joint angle error of **second** was better than **first**, because **second** uses the current muscle tension. The joint angle error of **proposed** was almost the same with **second**. Muscle tension of **geometric** was much lower than those using other methods. This is considered to be due to the loosening of muscles, since the difference between the actual robot and its geometric model is large and the control using the geometric model could not realize target joint angles. Muscle tension was likely to rise in **second** compared to in **first**. On the other hand, $\|T_{current}\|_2$ in **proposed** was lower than **first** and **second** at all θ_{eval} .

Because **first** and **second** are executed in order, it takes a long time to realize the target joint angles, and high internal muscle tension emerges. On the other hand, **proposed** can inhibit internal muscle tension and can realize the same tracking ability as **second**.

D. Simulation Using Musculoskeletal AutoEncoder

We conducted experiments of simulation using MAE. We show the difference of movements among the actual robot, simulation before online learning, and simulation after online learning in Fig. 11. The higher the muscle tension is, the redder its color becomes, and the lower the muscle tension is, the greener its color becomes. Compared to before online learning, we can see that the actual sensor values of joint angles and muscle tensions are close to the simulation after online learning. We show the transition of $\|\theta_{sim} - \theta_{current}\|_2$ and $\|T_{sim} - T_{current}\|_2$ before and after online learning in Fig. 12. We can see that the error between the actual sensor value and simulation value becomes smaller after online learning than before online learning, e.g. regarding joint angles, from 0.335 [rad] to 0.162 [rad] on average, and regarding muscle tensions, from 105 [N] to 92.2 [N] on average. Thus, we can make the simulator closer to the actual robot by learning.

Also, we show that the behavior of simulation can be altered by changing loss function, as stated in Section III-F,

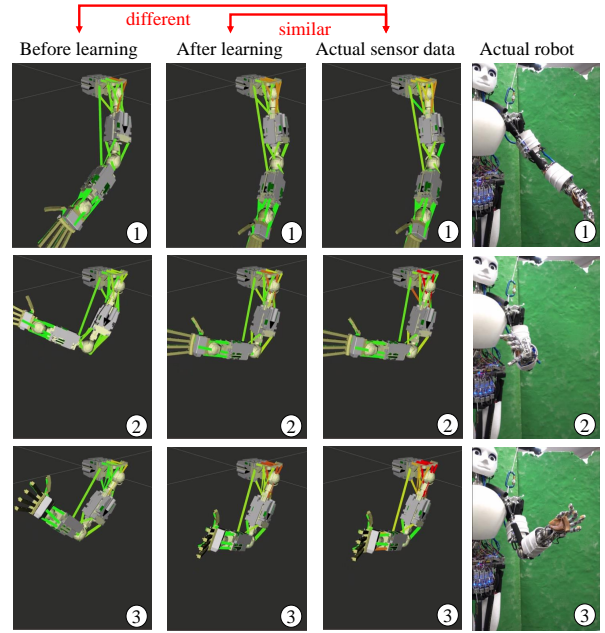


Fig. 11. The differences among the actual robot, simulation before online learning, and simulation after online learning.

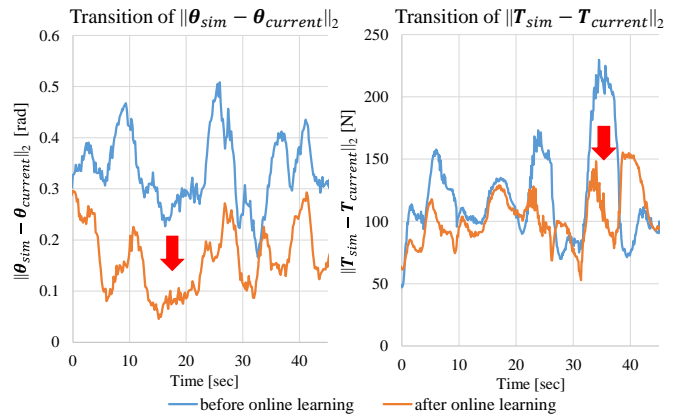


Fig. 12. The transition of $\|\theta_{sim} - \theta_{current}\|_2$ and $\|T_{sim} - T_{current}\|_2$ before and after online learning.

in Fig. 13. We conducted the movements of bending the elbow to 90 deg, applying external force of -50 N in z direction and 50 N in y direction in order, and changing θ_{s-p} to 30 deg forcibly by external force. When applying external force, we use the loss of Eq. 13, and when changing the posture forcibly, we use the loss of Eq. 14. By changing the applied force or setting θ_{fix} in Eq. 14, we can check the transitions of joint angles and muscle tensions. In the future, we would like to make use of the simulator for motion generation.

V. CONCLUSION

In this study, we proposed Musculoskeletal AutoEncoder (MAE) that uniformly handles state estimation, control, and simulation of musculoskeletal humanoids. MAE is an AutoEncoder-type network representing the relationship among joint angles, muscle lengths, and muscle tensions, which are equipped with the ordinary musculoskeletal humanoid, and we update it online using the actual robot

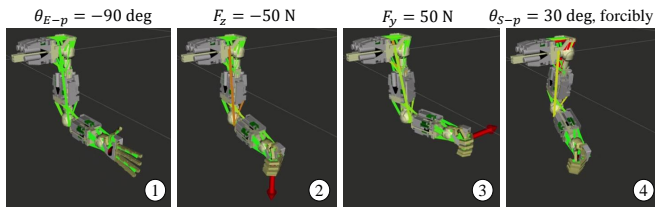


Fig. 13. The result of simulation experiment when changing the loss function.

sensor information. For state estimation, we can estimate the current joint angle by feeding the current muscle tension and length into MAE, and can also detect anomaly from whether the input values can be restored by MAE. For muscle length-based control, we can obtain the target muscle length to realize the target joint angle and minimize muscle tension by backpropagation of MAE. For simulation of joint angles and muscle tensions, we can calculate them to fulfill the necessary muscle length and joint torque by real-time backpropagation. Also, we can conduct muscle tension-based control and variable stiffness control by calculating muscle Jacobian from MAE. By using this study, we can integrate indispensable system components of musculoskeletal humanoids, and reflect the actual robot information to the model.

In future works, we would like to investigate the control and simulation techniques of musculoskeletal humanoids for dynamic movements.

REFERENCES

- [1] Y. Nakanishi, S. Ohta, T. Shirai, Y. Asano, T. Kozuki, Y. Kakehashi, H. Mizoguchi, T. Kurotobi, Y. Motegi, K. Sasabuchi, J. Urata, K. Okada, I. Mizuuchi, and M. Inaba, "Design Approach of Biologically-Inspired Musculoskeletal Humanoids," *International Journal of Advanced Robotic Systems*, vol. 10, no. 4, pp. 216–228, 2013.
- [2] S. Wittmeier, C. Alessandro, N. Bascarevic, K. Dalamagkidis, D. Devereux, A. Diamond, M. Jäntsch, K. Jovanovic, R. Knight, H. G. Marques, P. Milosavljevic, B. Mitra, B. Svetozarevic, V. Potkonjak, R. Pfeifer, A. Knoll, and O. Holland, "Toward Anthropomimetic Robotics: Development, Simulation, and Control of a Musculoskeletal Torso," *Artificial Life*, vol. 19, no. 1, pp. 171–193, 2013.
- [3] M. Jäntsch, S. Wittmeier, K. Dalamagkidis, A. Panos, F. Volkart, and A. Knoll, "Anthrob - A Printed Anthropomimetic Robot," in *Proceedings of the 2013 IEEE-RAS International Conference on Humanoid Robots*, 2013, pp. 342–347.
- [4] Y. Asano, T. Kozuki, S. Ookubo, M. Kawamura, S. Nakashima, T. Katayama, Y. Iori, H. Toshinori, K. Kawaharazuka, S. Makino, Y. Kakiuchi, K. Okada, and M. Inaba, "Human Mimetic Musculoskeletal Humanoid Kengoro toward Real World Physically Interactive Actions," in *Proceedings of the 2016 IEEE-RAS International Conference on Humanoid Robots*, 2016, pp. 876–883.
- [5] S. Ookubo, Y. Asano, T. Kozuki, T. Shirai, K. Okada, and M. Inaba, "Learning Nonlinear Muscle-Joint State Mapping Toward Geometric Model-Free Tendon Driven Musculoskeletal Robots," in *Proceedings of the 2015 IEEE-RAS International Conference on Humanoid Robots*, 2015, pp. 765–770.
- [6] Y. Nakanishi, K. Hongo, I. Mizuuchi, and M. Inaba, "Joint proprioception acquisition strategy based on joints-muscles topological maps for musculoskeletal humanoids," in *Proceedings of the 2010 IEEE International Conference on Robotics and Automation*, 2010, pp. 1727–1732.
- [7] Y. Motegi, T. Shirai, T. Izawa, T. Kurotobi, J. Urata, Y. Nakanishi, K. Okada, and M. Inaba, "Motion control based on modification of the Jacobian map between the muscle space and work space with musculoskeletal humanoid," in *Proceedings of the 2012 IEEE-RAS International Conference on Humanoid Robots*, 2012, pp. 835–840.
- [8] I. Mizuuchi, Y. Nakanishi, T. Yoshikai, M. Inaba, H. Inoue, and O. Khatib, "Body Information Acquisition System of Redundant Musculo-Skeletal Humanoid," in *Experimental Robotics IX*, 2006, pp. 249–258.
- [9] K. Kawaharazuka, S. Makino, M. Kawamura, Y. Asano, K. Okada, and M. Inaba, "Online Learning of Joint-Muscle Mapping using Vision in Tendon-driven Musculoskeletal Humanoids," *IEEE Robotics and Automation Letters*, vol. 3, no. 2, pp. 772–779, 2018.
- [10] K. Kawaharazuka, S. Makino, M. Kawamura, A. Fujii, Y. Asano, K. Okada, and M. Inaba, "Online Self-body Image Acquisition Considering Changes in Muscle Routes Caused by Softness of Body Tissue for Tendon-driven Musculoskeletal Humanoids," in *Proceedings of the 2018 IEEE/RSJ International Conference on Intelligent Robots and Systems*, 2018, pp. 1711–1717.
- [11] K. Kawaharazuka, K. Tsuzuki, S. Makino, M. Onitsuka, Y. Asano, K. Okada, K. Kawasaki, and M. Inaba, "Long-time Self-body Image Acquisition and its Application to the Control of Musculoskeletal Structures," *IEEE Robotics and Automation Letters*, vol. 4, no. 3, pp. 2965–2972, 2019.
- [12] A. Diamond and O. E. Holland, "Reaching control of a full-torso, modelled musculoskeletal robot using muscle synergies emergent under reinforcement learning," *Bioinspiration & Biomimetics*, vol. 9, no. 1, pp. 1–16, 2014.
- [13] S. Wittmeier, M. Jäntsch, K. Dalamagkidis, M. Rickert, H. G. Marques, and A. Knoll, "CALIPER: A universal robot simulation framework for tendon-driven robots," in *Proceedings of the 2011 IEEE/RSJ International Conference on Intelligent Robots and Systems*, 2011, pp. 1063–1068.
- [14] D. Lau, J. Eden, Y. Tan, and D. Oetomo, "CASPR: A comprehensive cable-robot analysis and simulation platform for the research of cable-driven parallel robots," in *Proceedings of the 2016 IEEE/RSJ International Conference on Intelligent Robots and Systems*, 2016, pp. 3004–3011.
- [15] S. Trendel, Y. P. Chan, A. Kharchenko, R. Hostettler, A. Knoll, and D. Lau, "CARDSFlow: An End-to-End Open-Source Physics Environment for the Design, Simulation and Control of Musculoskeletal Robots," in *Proceedings of the 2018 IEEE-RAS International Conference on Humanoid Robots*, 2018, pp. 245–250.
- [16] H. Kobayashi, K. Hyodo, and D. Ogane, "On Tendon-Driven Robotic Mechanisms with Redundant Tendons," *The International Journal of Robotics Research*, vol. 17, no. 5, pp. 561–571, 1998.
- [17] R. Niiyama, S. Nishikawa, and Y. Kuniyoshi, "Athlete Robot with applied human muscle activation patterns for bipedal running," in *Proceedings of the 2010 IEEE-RAS International Conference on Humanoid Robots*, 2010, pp. 498–503.
- [18] K. Kawaharazuka, S. Makino, K. Tsuzuki, M. Onitsuka, Y. Nagamatsu, K. Shinjo, T. Makabe, Y. Asano, K. Okada, K. Kawasaki, and M. Inaba, "Component Modularized Design of Musculoskeletal Humanoid Platform Musashi to Investigate Learning Control Systems," in *Proceedings of the 2019 IEEE/RSJ International Conference on Intelligent Robots and Systems*, 2019, pp. 7294–7301.
- [19] J. Urata, Y. Nakanishi, A. Miyadera, I. Mizuuchi, T. Yoshikai, and M. Inaba, "A Three-Dimensional Angle Sensor for a Spherical Joint Using a Micro Camera," in *Proceedings of the 2006 IEEE International Conference on Robotics and Automation*, 2006, pp. 4428–4430.
- [20] G. E. Hinton and R. R. Salakhutdinov, "Reducing the Dimensionality of Data with Neural Networks," *Science*, vol. 313, no. 5786, pp. 504–507, 2006.
- [21] D. P. Kingma and J. Ba, "Adam: A Method for Stochastic Optimization," in *Proceedings of the 3rd International Conference on Learning Representations*, 2015.
- [22] T. Shirai, J. Urata, Y. Nakanishi, K. Okada, and M. Inaba, "Whole body adapting behavior with muscle level stiffness control of tendon-driven multi-joint robot," in *Proceedings of the 2011 IEEE International Conference on Robotics and Biomimetics*, 2011, pp. 2229–2234.
- [23] D. E. Rumelhart, G. E. Hinton, and R. J. Williams, "Learning representations by back-propagating errors," *nature*, vol. 323, no. 6088, pp. 533–536, 1986.
- [24] M. Kawamura, S. Ookubo, Y. Asano, T. Kozuki, K. Okada, and M. Inaba, "A Joint-Space Controller Based on Redundant Muscle Tension for Multiple DOF Joints in Musculoskeletal Humanoids," in *Proceedings of the 2016 IEEE-RAS International Conference on Humanoid Robots*, 2016, pp. 814–819.